Mosquito cellular immunity at single-cell resolution

Gianmarco Raddi[1, 2, 3*], Ana Beatriz F Barletta[2*], Mirjana Efremova[1], Jose Luis Ramirez[2, 4], Rafael Cantera[5], Sarah A. Teichmann[1, 6], Carolina Barillas-Mury[2#], Oliver Billker[1, 7#]

[1] Wellcome Sanger Institute, Hinxton, Cambridge CB10 2AZ, UK.

[2] Laboratory of Malaria and Vector Research, National Institute of Allergy and Infectious Diseases, National Institutes of Health, Rockville, MD 20852, USA.

[3] Current affiliation: School of Clinical Medicine, University of Cambridge, Cambridge CB2 0SP, UK.

[4] Current affiliation: Crop Bioprotection Research Unit, United States Department of Agriculture, National Center for Agricultural Utilization Research, Agricultural Research Service, Peoria, IL, United States.

[5] Zoology Department, Stockholm University, Stockholm, S-10691, Sweden and Departamento de Biología del Neurodesarrollo, Instituto de Investigaciones Biológicas Clemente Estable, Montevideo 11600, Uruguay

[6] Institute & Dept Physics, University of Cambridge, JJ Thomson Ave, Cambridge CB3 0HE, UK.

[7] Molecular Infection Medicine Sweden, Molecular Biology Department, Umeå University, Umeå S-90187, Sweden.

[*] Contributed equally.

[#] To whom correspondence should be addressed: cbarillas@niaid.nih.gov, oliver.billker@umu.se

Hemocytes limit the capacity of mosquitoes to transmit human pathogens. Here we profile the transcriptomes of 8506 hemocytes of *Anopheles gambiae* and *Aedes aegypti* mosquito vectors. This revealed functional diversity of hemocytes, with different subtypes of granulocytes expressing distinct and evolutionarily conserved subsets of effector genes. A new cell type in *A. gambiae,* which we term megacyte, is defined by a unique transmembrane protein marker (TM7318) and high expression of LPS-Induced TNF-alpha transcription factor 3 (LL3). Knock-down experiments indicate that LL3 mediates hemocyte differentiation during immune priming. We identify and validate two main hemocyte lineages and find evidence of proliferating granulocyte populations. This atlas of medically relevant invertebrate immune cells at single cell resolution identifies cellular events that underpin mosquito immunity to malaria infection.

Anopheline mosquitoes transmit *Plasmodium* parasites to humans, and are responsible for an estimated 219 million cases of malaria, leading to over 400,000 deaths annually (*1*). Parasites taken up by female mosquitoes from the blood of an infected human transform into motile ookinetes, which traverse the mosquito midgut and establish an infection. The mosquito's immune system limits *Plasmodium* infection in several ways (2-4), and hemocytes, the insect white blood cells, are key players in these defense responses (5, 6). Ookinete invasion triggers a strong nitration response in invaded midgut epithelial cells and their basal lamina (7, 8). Hemocytes that come in contact with a nitrated midgut basal lamina release microvesicles into the epithelial basal labyrinth and promote local complement activation, inducing parasite lysis (6). An infection with *Plasmodium* primes mosquitoes to mount a stronger immune response to subsequent infections (9). Primed mosquitoes release hemocyte differentiation factor (HDF) into the hemolymph (9), consisting of a complex of lipoxin A4 bound to evokin, a lipocalin carrier (*10*). HDF increases the proportion of circulating hemocytes of the granulocyte type (2) promotes microvesicle release, and enhances complement-mediated parasite lysis (6). Enhanced immunity is lost if HDF synthesis is blocked (*10*).

Three hemocyte types have been described in *Anopheles gambiae* morphologically (*11*). Granulocytes are highly phagocytic cells of about 10-20 µm in diameter. Oenocytoids are 8-12 µm round cells that produce melanin, an insoluble pigment involved in wound healing and pathogen containment by encapsulation. Prohemocytes are round cells 4-6 µm with a high nuclear to cytoplasmic ratio, thought to be precursors of the other two cell types. Hemocytes alternate between circulatory and tissue-resident (sessile) states (*12*, *13*). However, the full functional diversity of mosquito hemocytes and their developmental trajectories have not been established, and it is not clear to what extent morphologically similar hemocytes are functionally equivalent.

Here, we use single-cell RNA sequencing (scRNA-seq) to analyze the transcriptional profile of individual mosquito hemocytes in response to blood feeding or infection with *Plasmodium*. Circulating hemocytes were collected from adult *A. gambiae* M form (*A. coluzzii*) females that were either kept on a sugar meal or fed on a healthy or a *Plasmodium berghei*-infected mouse (Fig. 1a). Transcriptomes from 5,383 cells (collected 1, 3, and 7 days after feeding) revealed nine major cell clusters (Figs. 1b, and S1). Two clusters originate from adipose tissue (fat body, FBC 1 and 2) and one from muscle tissue (MusC; Fig. 1b-c). FBC1 cells express several immune-modulatory genes such as CLIPs (CLIPA1, 7, 8, 9, 14), LRIMs (LRIM 1, 4A, 8A, 8B, 9, 17), lectins (CTL 4, MA2) and SRPN2 (Figs. 1b-c and S2, Table S1), while FBC2 cells express high levels of vitellogenin after blood feeding, a canonical fat body marker (*14*). On the basis of their unique transcriptional profiles, we identified six hemocyte clusters (HC) (Fig. 1b, c). Hemocyte cluster 1 (HC1) has high mRNAs levels of prophenoloxidases, including PPO4 (Figs. 1b-c) and PPO9, characteristic of oenocytoids. This expression profile agrees with reported scRNA-seq data for 25 hemocytes (*15*). To select markers for major hemocyte lineages, we used bulk RNAseq data from different tissues to identify hemocyte-specific genes (Fig. S3 and Table S2-3). HC1 contains low levels of leucine-repeat protein 8 (LRR8) mRNA, while HC2-4 have an inverse pattern (i.e. low or absent PPO4 and high LLR8 levels; Figs. 1b-c and 2a, and S2).

In situ hybridization using PPO4 and LLR8 as markers revealed that the morphology of circulating HC1 ($PPO4^{high}/LLR8^{low}$) cells is typical of oenocytoids, with round cells that have few pseudopodia and granules (Fig. 2b); while the morphology of HC2-4 ($PPO4^{low}/LLR8^{high}$) cells is typical of prohemocytes and granulocytes (Fig. 2b). HC2 and HC3 shared markers such as SPARC, cathepsin-L and LRR8 (Fig. 1c). However, HC2 had 73% fewer unique molecular identifiers (UMI) (mean UMI of 413) in comparison to HC3 (mean UMI of 1,516), suggesting that HC2 cells are less differentiated and probably constitute prohemocytes. Our observation that cells of prohemocyte morphology did not express markers of the more differentiated HC1 or HC5 cells is consistent with this notion (Fig. 2b). HC3 cells have a typical granulocyte morphology, with prominent pseudopodia and abundant granules (Fig. 2b).

HC4 shares markers with HC3, and a correlation analysis shows these cells to be granulocytes (Fig. S6c). However, HC3 cells are also characterized by a unique subset of markers (Fig. 1c). HC4 cells express cyclin B, aurora kinase and other mitotic markers, suggesting that they are proliferating hemocytes (Fig. S6c-e). Cells in HC5 and HC6 both are negative for PPO4 (Figs. 1c, 2a). HC5 cells express high levels of an uncharacterized transmembrane protein AGAP007318 (TM7318) and LPS-induced TNF-alpha transcription factor 3 (LL3) (Figs. 1c, 2a), while HC6 is negative for those markers and expresses antimicrobial peptides such as defensin 1, cecropins 1 and C-type lysozyme (Figs. 1c). Cells in HC5 and HC6 are both $LLR8^{low}$ and PPO4-negative but have two distinct morphologies (Fig. 2a-b). Cells negative for TM7318 (HC6) are small granulocytes that express antimicrobial genes (AM Gran) (16.4% of granulocytes), while TM7318 positive cells (HC5) are in low abundance (0.5% of granulocytes) and represent a separate giant cell type (25-40 µm) that we named “megacytes” (Fig. 2b).

To investigate the differentiation dynamics of *A. gambiae* hemocytes, we re-clustered the cellular transcriptomes at higher resolution and performed lineage-tree reconstruction with partition-based graph abstraction (PAGA)(*16*). The major granulocyte population sub-clustered into three cell populations representing a basal, homeostatic state (Gran1), and two states activated by blood-feeding and *Plasmodium*-infection (Gran2 and Gran3), (Fig. 2c, S6a-b). Prohemocytes were subclustered into two populations (PHem1 and PHem2), of which PHem2

appeared to be an intermediate stage between PHem1 and Gran1. We traced a connection between dividing granulocytes (Div Gran) and Gran3 granulocytes, which in turn link to Gran1. Gran1 also links to Gran2, which in turn links to megacytes (Megac), while Gran1 links directly to antimicrobial granulocytes (AM Gran; Fig. 2d). These findings were confirmed with the diffusion maps and slingshot cell-trajectory analysis packages (Fig. S4 and S5). Together, these analyses suggest the existence of a proliferative, oligopotent cell population that can replenish the pool of granulocytes and differentiate into more specialized hemocytes, such as megacytes and antimicrobial granulocytes.

Granulocytes (HC4 subtype) specifically express mitotic markers (Fig. S6c-e) largely in response to blood feeding (Fig. S6a-b), in agreement with a recent report that blood feeding induced DNA synthesis in hemocytes (*17*). Our data suggests that granulocyte proliferation and prohemocyte differentiation both contribute to the observed increase in granulocyte numbers after blood feeding (*11*, *18*, *19*). However, the placement of prohemocytes in the granulocyte lineage tree should be treated with caution due to the paucity of unique markers.

Prohemocytes are proposed to be stem cell precursors of both granulocytes and oenocytoids (*11*). However, oenocytoids are transcriptionally disconnected from other hemocyte subtypes, and we did not observe transcriptional markers of cell proliferation in oenocytoids, suggesting they may represent a separate lineage which has its origin either in larval stages or in other adult tissues. Alternatively, oenocytoids could derive from granulocytes (Fig. 1b), but the differentiation rate may be very low when melanization responses are not elicited, which could result in too few cells at intermediate stages of differentiation to be captured in our transcriptomic analysis.

To assess which of the newly discovered putative cell types are shared between anopheline and culicine mosquitoes, we analyzed the transcriptomes of 3123 hemolymph cells from *A. aegypti*, a vector for several viral diseases including yellow fever, dengue, chikungunya and Zika. As with *Anopheles*, a dimensional reduction plot shows both canonical hemocytes and

other cell types with mostly fat body signatures (Fig. 3a and Fig S7). A cross-species correlation analysis reveals two clusters (AaHC1 and AaHC2) with conserved transcriptome signatures for oenocytoids (99% and 77% correlation, respectively, with AgHC1) (Fig. 3a-b) and different granulocyte types, including antimicrobial peptide expressing cells (94% with AgHC6), and proliferating granulocytes (87% with AgHC4) (Fig. 3a-b; Table S4). Granulocytes and prohemocytes are again positioned along a continuum of transcriptomic similarity, with four different cell states, including a proliferating S-phase granulocyte cluster (AaHC6) without a clear *Anopheles* equivalent (Fig. 3a-b). Granulocytes express laminins, leucine-rich repeat proteins, scavenger receptors, Toll receptor 5, and the transcription factor Rel2 (Fig. S8 and Table S5). However, megacytes (AgHC5) lack an obvious counterpart in *Aedes*, and their unique marker (TM7318) is only present in anophelines of the *Cellia* subgenus (malaria vectors in Africa and Asia, Fig. S9).

The transcription factor LL3 can be detected in granulocytes from *Plasmodium*-infected *A. gambiae,* and silencing LL3 expression disrupts priming (*20*). However, it is not clear whether LL3 is essential for HDF synthesis or for hemocytes to respond to HDF. We found that LL3 is highly expressed in megacytes (HC5) (Figs. 1c and 4a) and explored whether silencing LL3 affects the HDF response. Transfer of hemolymph from primed *A. gambiae* donors had HDF activity and elicited a strong priming response in control recipients injected with *lacZ* double stranded (ds) RNA, resulting in a prominent increase in circulating granulocytes, a modest increase in oenocytoids and a decrease in prohemocytes (Fig. 4b and Table S6-9). This response was abolished when LL3 expression was silenced in the recipients by injection of dsLL3 RNA (Fig. 4b and Table S6-9). We cannot rule out that hemocytes other than megacytes express LL3 at levels below the detection limit of scRNA-seq, which could have led to the notion that LL3 is upregulated more broadly in granulocytes after *Plasmodium* infection (*20*), in which case LL3 silencing might directly control hemocyte differentiation in response to HDF directly. However, the discovery of megacytes expressing high levels of LL3 as a defining feature now raises the intriguing possibility that it is this cell type which plays a key role in orchestrating hemocyte responses to HDF.

The proportion of circulating granulocytes is low (1-3%) under normal conditions but increases in response to *Plasmodium* infection (*2*). Whether the increase is due to granulocyte proliferation, differentiation from prohemocytes or to mobilization of sessile hemocytes was unknown. Transmission electron microscopy of sugar fed mosquitoes showed individual sessile hemocytes bathed by hemolymph and attached to the basal lamina of the tissues through pseudopods (Fig. 4c), indicative of a dynamic and potentially transient association.

Using whole tissue mount *in situ* hybridization we found that most sessile hemocytes are $PPO4^{low}/LLR8^{high}$ granulocytes (89.3 ± 6.2% SEM), while $PPO4^{high}/LLR8^{low}$ oenocytoids are less abundant (4.2 ± 3.1% SEM) and TM7318 positive megacytes are even rarer (2.7 ± 2.3% SEM) (Fig. 4d-e and Table S10-11). Furthermore, we found a reduction of sessile $PPO4^{low}/LLR8^{high}$ granulocytes in response to *Plasmodium* infection ($P<0.0001$, Welch T-Test, Fig. 4e and Table S12-13), with no significant difference in the numbers of sessile $PPO4^{high}/LLR8^{low}$ oenocytoids, $TM7318^{+}$ megacytes or $TM7318^{-}$ AM granulocytes (Fig. 4e and Table S12-13). In circulating hemocytes, *P. berghei* infection induced high expression of a fibrinogen-like protein AGAP029831 (FBN29831) (Fig. S10). RNA *in situ* hybridization showed that the proportion of FBN29831-positive cells increased in both $PPO^{low}/LLR8^{high}$ granulocytes ($P<0.0001$, X^2, Fig. 4f and Table S14-15) and $PPO4^{high}/LLR8^{low}$ oenocytoids ($P<0.0001$, X^2, Fig. 4g and Table S16-17), indicating that this is a general marker of hemocyte immune activation. Infecting *A. gambiae* with the human parasite *P. falciparum* produced a similar increase in FBN29831-positive cells (Fig. S11). Combined, our results suggest that hemocyte recruitment from the body wall, granulocyte activation and proliferation, and prohemocyte differentiation can all contribute to boost circulating granulocyte numbers upon immune challenge.

The hemocyte atlas presented here confirms the existence of two canonical hemocyte types in mosquitoes, the oenocytoids and granulocytes, and with the help of transcript markers we relate cellular morphology to their transcriptome. We show prohemocytes and granulocytes to be closely related cells, and identified transcriptional profiles and molecular markers that define

previously unknown hemocyte subtypes (megacytes, proliferating granulocytes, and antimicrobial granulocytes), as well as a subpopulation of fat body cells (AgFBC1) with potential immune-modulatory functions.

We define two main hemocyte lineages in *A. gambiae*: the oenocytoid lineage, and the prohemocyte-granulocyte lineage along with three sub lineages leading to differentiated megacytes, antimicrobial granulocytes, or proliferating granulocytes. The cell-type markers and FISH probes we identify and validate will allow investigators to probe the immune functions of megacytes and other specialized hemocyte types in detail, which will provide a basis for a better understanding of how cellular immunity limits the ability of malaria parasites to infect mosquitoes. Our analysis cannot resolve the developmental origin of oenocytoids, but we identify two potential origins for the observed expansion of circulating granulocytes upon blood feeding. One is the mobilization of sessile PPO4^{low}/LLR8^{high} cells from the body wall, the other is a pool of proliferating, oligopotent granulocytes. Whether prohemocytes, which appear transcriptionally related to, but less responsive than granulocytes, can transform into granulocytes and whether they need to enter the cell cycle, remains to be determined. These questions may now be addressed with the type of lineage tracing experiments commonly performed in mouse immunology to resolve the developmental origins and functions of diverse immune cell populations. The cell-type-specific marker genes, reference transcriptomes, and companion website (https://hemocytes.cellgeni.sanger.ac.uk/) we present here will serve as a resource for such studies.

The conservation of diverse and molecularly well-defined hemocyte types between distantly related mosquito genera and the apparent absence of megacytes in our *A. aegypti* mosquito dataset raise interesting questions as to how the immune systems of these mosquito species have evolved to limit their capacity to transmit parasites and arboviruses to humans. This knowledge will ultimately underpin immunological strategies aimed at interrupting disease transmission by rendering mosquitoes resistant to such pathogens.

References

1 WHO, *World malaria report 2019* (https://www.who.int/publications-detail/world-malaria-report-2019).

2 J. Rodrigues, F. A. Brayner, L. C. Alves, R. Dixit, C. Barillas-Mury, Hemocyte differentiation mediates innate immune memory in Anopheles gambiae mosquitoes. *Science*. **329**, 1353–1355 (2010).

3 S. Luckhart, Y. Vodovotz, L. Cui, R. Rosenberg, The mosquito Anopheles stephensi limits malaria parasite development with inducible synthesis of nitric oxide. *Proc. Natl. Acad. Sci. U. S. A.* **95**, 5700–5705 (1998).

4 S. Blandin, S.-H. Shiao, L. F. Moita, C. J. Janse, A. P. Waters, F. C. Kafatos, E. A. Levashina, Complement-like protein TEP1 is a determinant of vectorial capacity in the malaria vector Anopheles gambiae. *Cell*. **116**, 661–670 (2004).

5 J. L. Ramirez, L. S. Garver, F. A. Brayner, L. C. Alves, J. Rodrigues, A. Molina-Cruz, C. Barillas-Mury, The role of hemocytes in Anopheles gambiae antiplasmodial immunity. *J. Innate Immun.* **6**, 119–128 (2014).

6 J. C. Castillo, A. B. B. Ferreira, N. Trisnadi, C. Barillas-Mury, Activation of mosquito complement antiplasmodial response requires cellular immunity. *Sci. Immunol.* **2** (2017), doi:10.1126/sciimmunol.aal1505.

7 S. Kumar, L. Gupta, Y. S. Han, C. Barillas-Mury, Inducible peroxidases mediate nitration of Anopheles midgut cells undergoing apoptosis in response to Plasmodium invasion. *J. Biol. Chem.* **279**, 53475–53482 (2004).

8 G. de A. Oliveira, J. Lieberman, C. Barillas-Mury, Epithelial nitration by a peroxidase/NOX5 system mediates mosquito antiplasmodial immunity. *Science*. **335**, 856–859 (2012).

9 B. C. Ho, E. H. Yap, M. Singh, Melanization and encapsulation in Aedes aegypti and Aedes togoi in response to parasitization by a filarioid nematode (Breinlia booliati). Parasitology. 85 (Pt 3), 567–575 (1982).

10 J. L. Ramirez, G. de Almeida Oliveira, E. Calvo, J. Dalli, R. A. Colas, C. N. Serhan, J. M. Ribeiro, C. Barillas-Mury, A mosquito lipoxin/lipocalin complex mediates innate immune priming in Anopheles gambiae. *Nat. Commun.* **6**, 7403 (2015).

11 J. C. Castillo, A. E. Robertson, M. R. Strand, Characterization of hemocytes from the mosquitoes Anopheles gambiae and Aedes aegypti. *Insect Biochem. Mol. Biol.* **36**, 891–903 (2006).

12 J. G. King, J. F. Hillyer, Infection-induced interaction between the mosquito circulatory and immune systems. *PLoS Pathog.* **8**, e1003058 (2012).

13 J. G. King, J. F. Hillyer, Spatial and temporal in vivo analysis of circulating and sessile immune cells in mosquitoes: hemocyte mitosis following infection. *BMC Biol.* **11**, 55 (2013).

14 G. M. Attardo, I. A. Hansen, A. S. Raikhel, Nutritional regulation of vitellogenesis in mosquitoes: implications for anautogeny. *Insect Biochem. Mol. Biol.* **35**, 661–675 (2005).

15 M. S. Severo, J. J. M. Landry, R. L. Lindquist, C. Goosmann, V. Brinkmann, P. Collier, A. E. Hauser, V. Benes, J. Henriksson, S. A. Teichmann, E. A. Levashina, Unbiased classification of mosquito blood cells by single-cell genomics and high-content imaging. *Proc. Natl. Acad. Sci. U. S. A.* **115**, E7568–E7577 (2018).

16 F. A. Wolf, F. K. Hamey, M. Plass, J. Solana, J. S. Dahlin, B. Göttgens, N. Rajewsky, L. Simon, F. J. Theis, PAGA: graph abstraction reconciles clustering with trajectory inference through a topology preserving map of single cells. *Genome Biol.* **20**, 59 (2019).

17 W. B. Bryant, K. Michel, Blood feeding induces hemocyte proliferation and activation in the African malaria mosquito, Anopheles gambiae Giles. *J. Exp. Biol.* **217**, 1238–1245 (2014).

18 L. A. Baton, A. Robertson, E. Warr, M. R. Strand, G. Dimopoulos, Genome-wide transcriptomic profiling of Anopheles gambiae hemocytes reveals pathogen-specific signatures upon bacterial challenge and Plasmodium berghei infection. *BMC Genomics*. **10**, 257 (2009).

19 J. Castillo, M. R. Brown, M. R. Strand, Blood feeding and insulin-like peptide 3 stimulate proliferation of hemocytes in the mosquito Aedes aegypti. *PLoS Pathog.* **7**, e1002274 (2011).

20 R. C. Smith, C. Barillas-Mury, M. Jacobs-Lorena, Hemocyte differentiation mediates the mosquito late-phase immune response against Plasmodium in Anopheles gambiae. *Proc. Natl. Acad. Sci. U. S. A.* **112**, E3412-3420 (2015).

21 Franke-Fayard, B. *et al.* A Plasmodium berghei reference line that constitutively expresses GFP at a high level throughout the complete life cycle. *Mol Biochem Parasitol* **137**, 23-33, doi:10.1016/j.molbiopara.2004.04.007 (2004).

22 Molina-Cruz, A. *et al.* Some strains of Plasmodium falciparum, a human malaria parasite, evade the complement-like system of Anopheles gambiae mosquitoes. *Proc Natl Acad Sci U S A* **109**, E1957-1962, doi:10.1073/pnas.1121183109 (2012).

23 Barletta, A. B. F., Trisnadi, N., Ramirez, J. L. & Barillas-Mury, C. Mosquito Midgut Prostaglandin Release Establishes Systemic Immune Priming. *iScience* **19**, 54-62, doi:10.1016/j.isci.2019.07.012 (2019).

24 Livak, K. J. & Schmittgen, T. D. Analysis of relative gene expression data using real-time quantitative PCR and the 2(-Delta Delta C(T)) Method. *Methods* **25**, 402-408, doi:10.1006/meth.2001.1262 (2001).

25 Pfaffl, M. W. A new mathematical model for relative quantification in real-time RT-PCR. *Nucleic Acids Res* **29**, e45, doi:10.1093/nar/29.9.e45 (2001).

26 Love, M. I., Huber, W. & Anders, S. Moderated estimation of fold change and dispersion for RNA-seq data with DESeq2. *Genome Biol* **15**, 550, doi:10.1186/s13059-014-0550-8 (2014).

27 Zheng, G. X. *et al.* Massively parallel digital transcriptional profiling of single cells. *Nat Commun* **8**, 14049, doi:10.1038/ncomms14049 (2017).

28 Giraldo-Calderon, G. I. *et al.* VectorBase: an updated bioinformatics resource for invertebrate vectors and other organisms related with human diseases. *Nucleic Acids Res* **43**, D707-713, doi:10.1093/nar/gku1117 (2015).

29 Satija, R., Farrell, J. A., Gennert, D., Schier, A. F. & Regev, A. Spatial reconstruction of single-cell gene expression data. *Nat Biotechnol* **33**, 495-502, doi:10.1038/nbt.3192 (2015).

30 Stuart, T. *et al.* Comprehensive Integration of Single-Cell Data. *Cell* **177**, 1888-1902 e1821, doi:10.1016/j.cell.2019.05.031 (2019).

31 Butler, A., Hoffman, P., Smibert, P., Papalexi, E. & Satija, R. Integrating single-cell transcriptomic data across different conditions, technologies, and species. *Nat Biotechnol* **36**, 411-420, doi:10.1038/nbt.4096 (2018).

32 Haghverdi, L., Buttner, M., Wolf, F. A., Buettner, F. & Theis, F. J. Diffusion pseudotime robustly reconstructs lineage branching. *Nat Methods* **13**, 845-848, doi:10.1038/nmeth.3971 (2016).

33 Wolf, F. A., Angerer, P. & Theis, F. J. SCANPY: large-scale single-cell gene expression data analysis. *Genome Biol* **19**, 15, doi:10.1186/s13059-017-1382-0 (2018).

34 Qiu, X. *et al.* Reversed graph embedding resolves complex single-cell trajectories. *Nat Methods* **14**, 979-982, doi:10.1038/nmeth.4402 (2017).

35 Street, K. *et al.* Slingshot: cell lineage and pseudotime inference for single-cell transcriptomics. *BMC Genomics* **19**, 477, doi:10.1186/s12864-018-4772-0 (2018).

Acknowledgements: The authors are grateful to T. Metcalf for technical support, to A. Goldsborough for making available the vivoPHIX reagent and advising on its use, to J. Eliasova for help with illustrations, to the Wellcome Sanger Institute CellGen team for creating and maintaining the data-visualisation website. **Funding:** This work was funded by the Intramural Research Program of the Division of Intramural Research Z01AI000947, National Institute of Allergy and Infectious Diseases (NIAID), NIH to CBM, by an NIH Oxford-Cambridge fellowship and a UCLA-Caltech Medical Scientist Training Program grant (NIGMS T32 GM008042) to GR, a Wellcome core grant 206194/Z/17/Z to the Sanger Institute and funding from the Knut and Alice Wallenberg foundation and the European Research Council (Grant agreement No. 788516) to OB. **Author contributions:** Conceptualisation: G.R., A.B.F.B., M.E., S.A.T., C.B.-M., O.B.; Methodology: G.R.; Investigation: G.R., A.B.F.B., J.L.R., R.C. Formal analysis: G.R., A.B.F.B., M.E.; Writing - Original Draft G.R., C.B.-M., O.B.; Supervision: S.A.T., C.B.-M., O.B.; Funding acquisition: S.A.T., C.B.-M., O.B.; All authors reviewed the manuscript. **Competing interests:** SAT reports consulting and SAB activities in the last 3 years for Genentech, Roche, Biogen, GSK and Foresite Labs. Other authors declare no competing interests. **Data and materials availability:** scRNAseq data for *A. gambiae* and *A. aegypti* hemocytes are available in ArrayExpress under accession number E-MTAB-9240. Bulk RNAseq data is available under accession number E-MTAB-9241. The code to reproduce the analysis of the paper is available on Zenodo under accession number DOI: 10.5281/zenodo.3882128. All other data are available in the manuscript or the supplementary materials.

Supplementary Materials:

Materials and Methods

Figures S1-S11

Tables S3, S4, and S6 to S18

External Databases S1, S2, and S5

References (*21-35*)

Figure 1

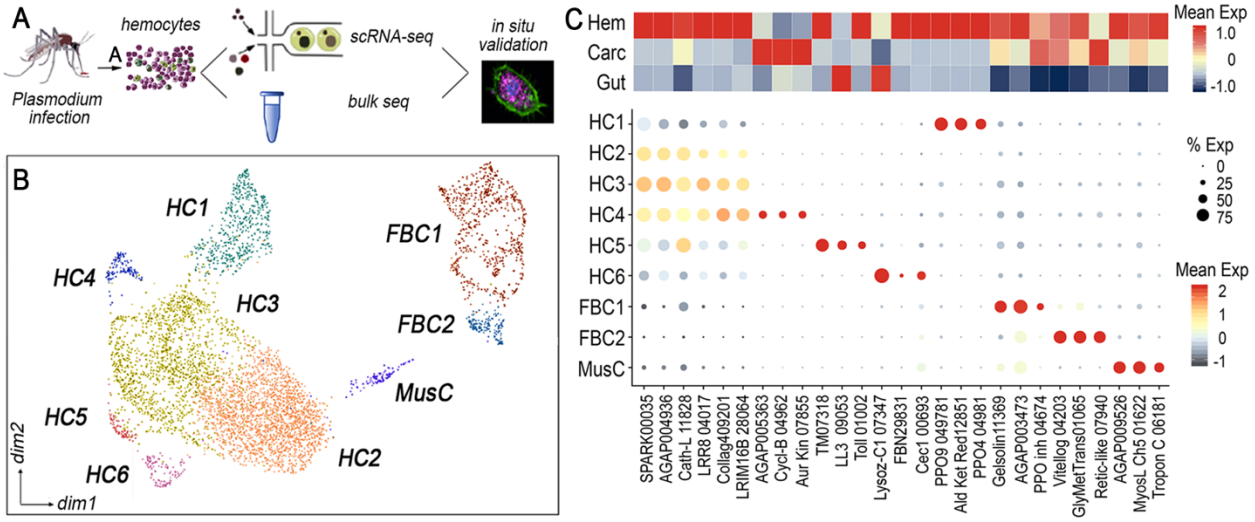

Fig. 1: Molecular identification of hemocyte cell types of *Anopheles* mosquitoes
a, Workflow and experimental scheme. **b**, UMAP of 5383 hemolymph *A. gambiae* (M-form) cells colored by cluster (cell type) identity with Seurat clustering. HC, hemocyte cluster; Mus, muscle; FBC, fat body cluster. **c**, Top panel: heatmap showing mean expression of three gene markers per scRNA-seq cluster in bulk-RNAseq of mosquito tissues. Hem, hemocytes; Carc, carcasses; Gut, gut samples. Bottom panel: dot plot showing corresponding expression of the cluster markers genes, where color indicates mean expression and dot size encodes percentage of cells within the cluster expressing the marker. Last five digits of each marker gene are the Vectorbase transcript accession numbers (after AGAP0).

Figure 2

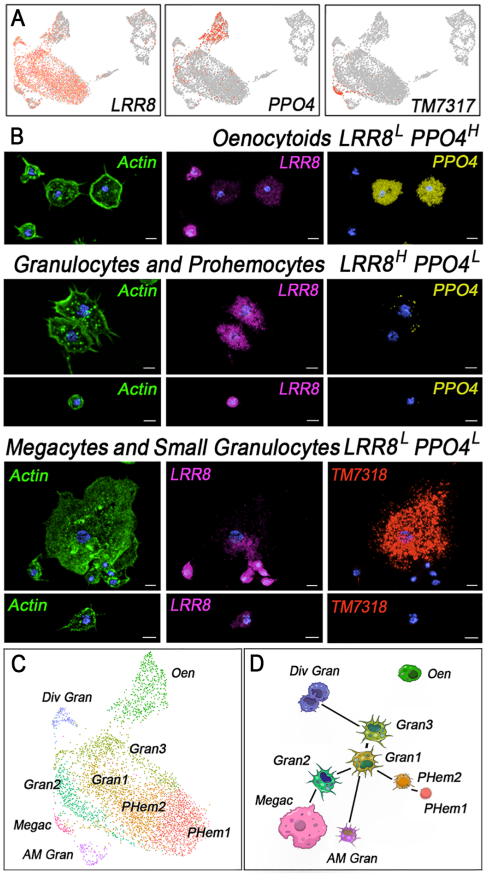

Fig. 2: Cell type validation and characterisation of *An. gambaie* hemocyte lineages
a, UMAP visualisation of marker gene expression. Cells with more than 1 UMI shown in red. **b**, RNA *in-situ* hybridization combined with morphology analysis of circulating hemocytes. Actin shown in green, LRR8 in magenta, PPO4 in yellow, TM7318 in red and nuclei in blue. Scale bar: 5 µm. **c**, UMAP of 5383 hemolymph cells colored by cluster (cell state) identity with Seurat clustering. **d**, Unsupervised partition-based graph abstraction (PAGA) network analysis connecting stylised cell states based on UMAP clustering. Oen, oenocytoids; Div Gran, dividing granulocytes; Gran, granulocytes; Megac, megacytes; AM Gran, antimicrobial granulocytes; PHem, prohemocytes.

Figure 3

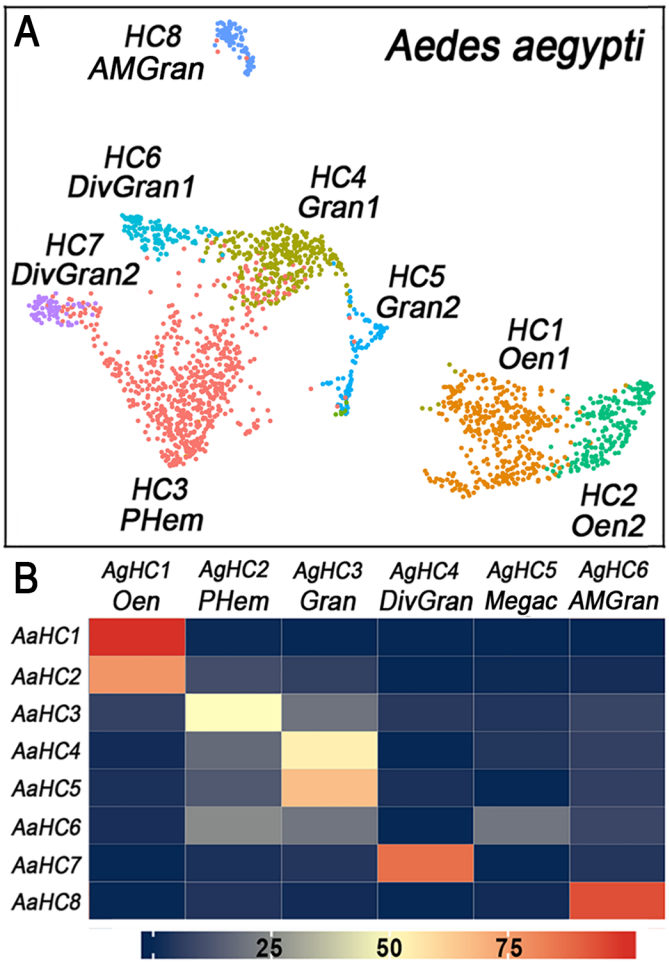

Fig. 3: Characterisation of *Aedes aegypti* hemocytes and correlation with *Anopheles* cell types
a, UMAP of 3123 *A. aegypti* hemocytes colored by cluster identity with Seurat. **b**, Heatmap showing probability of each *A. aegypti* hemocyte in a cluster belonging to each of the *A. gambiae* (M-form) cell types after logistic regression and using a multinomial learning approach. *Ag*, *A. gambiae* (M-form); *Aa*, *A. aegypti*. Oen, oenocytoids; Div Gran, dividing granulocytes; Gran, granulocytes; Mega, megacytes; AM Gran, antimicrobial granulocytes; PHem, prohemocytes.

Figure 4

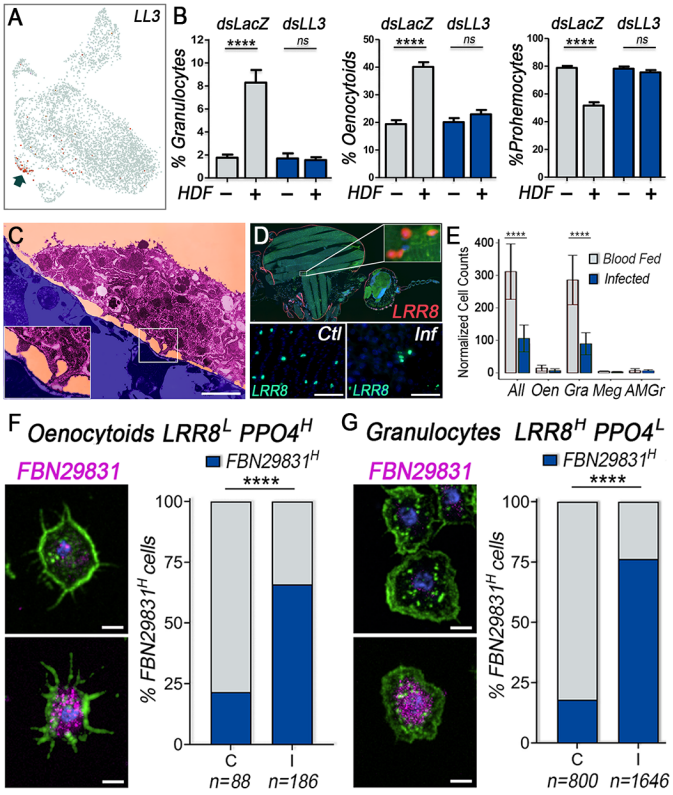

Fig. 4: *Anopheles gambiae* cellular immune responses to *Plasmodium* infection

a, UMAP visualisation of all hemocytes by *LL3* expression. Red indicates cells with more than 1 UMI. Arrow points at megacyte cluster. **b**, Percentage of circulating granulocytes, oenocytoids and prohemocytes of *LL3*-silenced mosquitoes injected (+) or not (-) with HDF versus double-stranded *lacZ* RNA injected mosquitoes used as negative controls (mean ± SEM, **** P<0.0001, unpaired t-test; two independent experiments). **c**, Transmission electron microscopy (TEM) in false colors depicting *A. gambiae* (M form) granulocyte (purple) attached via pseudopodia (insert) to the abdominal fat body (blue); scale bar: 1.5 µm. **d**, RNA *in-situ* hybridisation of a longitudinal section (top panel) or carcass whole-mounts (bottom panels) of control blood-feed (Ctl) and *P. berghei* (Inf) infected *A. gambiae* mosquitoes. Top panel: GAPDH in green, LRR8 in red. Bottom panels: LRR8 in green. Scale bar: 20 µm. **e**, Quantification of *Anopheles* hemocytes attached to the mosquito fat body with blood-feeding or *P. berghei* infection, normalised by surface area of fat bodies. RNA *in-situ* hybridisation of a longitudinal section (top panel) or carcass whole-mounts. All, all hemocytes; Oen, oenocytoids; Gran, granulocytes; AM Gran, antimicrobial granulocytes (mean ± SEM, **** P<0.0001, Welch T-test; three independent experiments). **f**, Percentage of circulating oenocytoids ($LRR^{L}PPO4^{H}$) and **g**, granulocytes ($LRR^{H}PPO4^{L}$) positive for *FBN29831* in control (C) and *P. berghei* infected (I) mosquitoes, 48 hours post feeding (right panels). Representative RNA *in-situ* hybridisation pictures of oenocytoids (**f**) and granulocytes (**g**) with low and high expression of FBN29831 (left panels). Actin in green, FBN29831 in magenta, nuclei in blue. Scale bar: 5 µm (****P<0.0001, Chi-square test; two independent experiments).